

Overcoming mTOR resistance mutations with a new-generation mTOR inhibitor

Vanessa S. Rodrik-Outmezguine^{1*}, Masanori Okaniwa^{2*}, Zhan Yao^{1*}, Chris J. Novotny², Claire McWhirter³, Arpitha Banaji¹, Helen Won⁴, Wai Wong⁵, Mike Berger⁴, Elisa de Stanchina⁵, Derek G. Barratt³, Sabina Cosulich³, Teresa Klinowska³, Neal Rosen^{1,6} & Kevan M. Shokat^{2,7}

Precision medicines exert selective pressure on tumour cells that leads to the preferential growth of resistant subpopulations, necessitating the development of next-generation therapies to treat the evolving cancer. The PIK3CA–AKT–mTOR pathway is one of the most commonly activated pathways in human cancers¹, which has led to the development of small-molecule inhibitors that target various nodes in the pathway. Among these agents, first-generation mTOR inhibitors (rapalogs) have caused responses in ‘N-of-1’ cases, and second-generation mTOR kinase inhibitors (TORKi) are currently in clinical trials^{2–4}. Here we sought to delineate the likely resistance mechanisms to existing mTOR inhibitors in human cell lines, as a guide for next-generation therapies. The mechanism of resistance to the TORKi was unusual in that intrinsic kinase activity of mTOR was increased, rather than a direct active-site mutation interfering with drug binding. Indeed, identical drug-resistant mutations have been also identified in drug-naïve patients, suggesting that tumours with activating *MTOR* mutations will be intrinsically resistant to second-generation mTOR inhibitors. We report the development of a new class of mTOR inhibitors that overcomes resistance to existing first- and second-generation inhibitors. The third-generation mTOR inhibitor exploits the unique juxtaposition of two drug-binding pockets to create a bivalent interaction that allows inhibition of these resistant mutants.

The MCF-7 breast cancer cell line was exposed to high concentrations of either a first-generation mTORC1 inhibitor, rapamycin or a second-generation mTOR ATP competitive inhibitor, AZD8055 (a TORKi), for 3 months, until resistant colonies emerged. Deep sequencing revealed that the AZD8055-resistant (TKi-R) clones harboured an *MTOR* mutation located in the kinase domain at the M2327I position (Fig. 1a and Extended Data Fig. 1a), while two rapamycin-resistant (RR) clones contained mutations located in the FKBP12–rapamycin-binding domain (FRB domain) at positions A2034V (RR1 cells) and F2108L (RR2 cells). The clinical relevance of these mutations is supported by a case report of a patient who acquired the identical F2108L *MTOR* mutation after relapse while under treatment with everolimus⁵ (Extended Data Table 1).

To verify that the mutations altered the efficacy of their respective drugs and were not simply passenger mutations, we analysed the phosphorylation of effectors downstream of mTOR in several cellular systems. In the RR cells, phosphorylation of the normally rapamycin-sensitive sites on S6K (T389) and S6 (S240/244 and S235/236) were unaffected even at high rapalog concentrations (100 nM) (Fig. 1b and Extended Data Fig. 1b). Phosphorylation of the key mTOR effector 4EBP1 is normally unaffected by rapamycin but strongly reduced by

TORKi^{6–8}. In the TKi-R cells, however, 4EBP1 phosphorylation was significantly less sensitive to a variety of TORKi (Fig. 1c and Extended Data Fig. 1c, d). Consistent with this weakened signalling inhibition, the RR and TKi-R clones were significantly less sensitive to their respective drugs in a 72 h proliferation assay when compared to the parental line (Fig. 1d, e and Supplementary Table 1). To determine if the RR and TKi-R *MTOR* mutations were directly responsible for the drug-resistance phenotype, each mutant was expressed in another model, MDA-MB-468 cells, which confirmed that the *MTOR* mutations are sufficient to promote dominant resistance (Extended Data Fig. 2a–d).

FRB domain mutations have been found in untreated patients (Extended Data Table 2), and previous random mutagenesis screens in yeast have shown that single amino acid changes in the mTOR FRB domain confer rapamycin resistance^{9–12}. The RR mutants identified in this screen exhibit a similar mechanism of resistance by disrupting the interaction of mTOR with the FKBP12–rapamycin complex in cells and *in vitro* (Fig. 2a, b).

In contrast to the FRB-domain mutations found in RR cells, which line the rapalog/FKBP-binding pocket, analysis of the recently solved structure of the mTOR kinase domain in complex with the TORKi, PP242 (Protein Data Bank (PDB), 4JT5)¹³, revealed that M2327 is >15 Å away from the inhibitor, suggesting either an allosteric mechanism of reduced TORKi affinity or that this mutation causes resistance through a mechanism that does not involve reduced drug binding. Indeed, both wild-type and M2327I mTOR bind AZD8055 with similar affinities (Fig. 2c). We asked whether the M2327I mutation in the mTOR kinase domain altered the kinetic properties of the kinase. As shown in Fig. 2d, the M2327I mutant has a threefold increase in mTOR kinase activity compared with the wild-type and RR mutants. This is consistent with the higher phosphorylated (p)-S6K (T389), p-AKT (S473) and p-4EBP1 S65 basal levels observed in these cells (Extended Data Fig. 1d).

The emergence of a hyperactive *MTOR* kinase domain mutation (M2327I) that could theoretically confer a growth advantage led us to wonder if similar mutations might pre-exist in drug-naïve patient tumours. Indeed, the precise M2327I mutation as well as other *MTOR* kinase domain mutations have been identified in five untreated patients (Extended Data Tables 1 and 3)^{14,15}. To determine if additional *MTOR* kinase domain mutants were also hyperactive and insensitive to TORKi, various *MTOR* kinase domain mutations that occur in patients were inducibly expressed in MDA-MB-468 cells and tested for sensitivity to the TORKi AZD8055 and MLN0128 (Extended Data Fig. 2d, e). The concentrations of drug required to inhibit mTORC1 and mTORC2 substrates in these cells were 3- to 30-fold higher than

¹Program in Molecular Pharmacology, Memorial Sloan-Kettering Cancer Center, New York, New York 10065, USA. ²Howard Hughes Medical Institute and Department of Cellular and Molecular Pharmacology, University of California San Francisco, San Francisco, California 94158, USA. ³AstraZeneca, Alderley Park, Macclesfield, Cheshire SK10 4TG, UK. ⁴Human Oncology and Pathogenesis Program, Memorial Sloan-Kettering Cancer Center, New York, New York 10065, USA. ⁵Anti-Tumor Assessment Core, Memorial Sloan Kettering Cancer Center, New York, New York 10065, USA. ⁶Department of Medicine, Memorial Sloan Kettering Cancer Center, New York, New York 10065, USA. ⁷Department of Chemistry, University of California Berkeley, Berkeley, California 94720, USA.

*These authors contributed equally to this work.

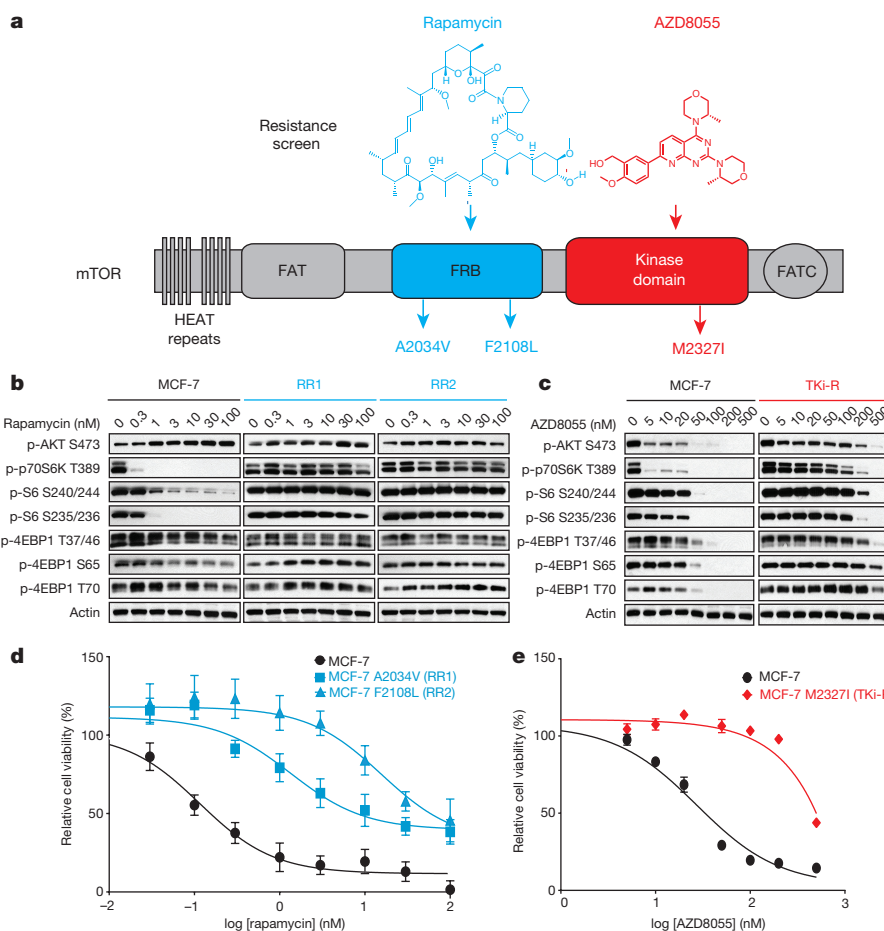


Figure 1 | Single amino acid mutation accounts for acquired resistance to mTOR inhibitors. **a**, Graphic representation of mTOR domains and site mutagenesis isolated in rapamycin- and AZD8055-resistant cells. **b, c**, The effects of rapamycin (**b**) or AZD8055 (**c**) on mTOR signalling was assessed in MCF-7, RR1 and RR2 cells (or in TKi-R cells (**c**) by immunoblotting 4 h after treatment. For gel source data, see Supplementary Fig. 1.

those required in wild-type cells, although not all substrates show precisely the same dose response.

These data suggest that the hyperactivation of mTOR kinase by single amino acid mutations found in drug-naïve patients can reduce the sensitivity to ATP-competitive mTOR inhibitors in cells. These findings highlight the need for a new class of mTOR inhibitor capable of targeting both drug-naïve (pre-existing) MTOR mutant-driven cancers, as well as emergent resistant mutations.

We developed a molecular model of mTOR in complex with rapamycin–FKBP12 using the FRB domain as the common domain in two available mTOR crystal structures (PDB, 1FAP and 4JT5) (Fig. 3a). This model revealed the juxtaposition of the rapamycin- and TORKi-binding sites and suggested an avidity-based approach to overcome drug-resistant mutations in either the FRB or the kinase domain. A bivalent mTOR inhibitor consisting of a rapamycin–FRB-binding element appropriately linked to a TORKi would be expected to inhibit the RR class of FRB-domain mutants because the TORKi-binding site would provide high-affinity recognition. For the TKi-R class of kinase domain mutations, a bivalent inhibitor would be predicted to be similarly potent by virtue of an intact rapamycin-binding site. We reasoned that binding at one site would position the second half of the ligand in close proximity for binding to the second site, thus overcoming point mutations that diminish drug binding (as found in RR cells) or that hyperactivate the kinase (as found in TKi-R cells)¹⁶. To develop a new bivalent class of mTOR inhibitors, we required a non-perturbing, strain-free linker between rapamycin and a TORKi,

d, e, Dose-dependent cell growth inhibition curves of MCF-7 and rapamycin-resistant MCF-7 A2034V (RR1) and MCF-7 F2108L (RR2) cells treated with rapamycin at day 3 (**d**) or MCF-7 and AZD8055-resistant MCF-7 M2327I (TKi-R) cells treated with AZD8055 (**e**). Each dot and error bar on the curves represents mean \pm standard deviation (s.d.) ($n=8$). All experiments were repeated at least three times.

such that the resulting inhibitor can simultaneously bind to both sites. Analysis of our mTOR–rapamycin–FKBP12 model revealed that the hydroxyl group at the C40 position of rapamycin is exposed to solvent and is oriented towards the ATP-binding site of mTOR (Fig. 3a). Analysis of the TORKi (PP242)-bound structure (PDB, 4JT5) revealed that the N-1 position of the pyrazole ring is oriented towards rapamycin and exposed to solvent (Extended Data Fig. 3a). We selected MLN0128 as the TORKi as it is a highly selective¹⁷ structural analogue of PP242, and is currently in clinical trials.

To determine the optimum linker length between the chosen sites, we used the molecular modelling program Molecular Operating Environment¹⁸ to evaluate the potential energy of a methylene-based cross-linker with lengths from 10 to 40 heavy atoms. This analysis revealed that 27 atoms would be the minimal length required to span the two ligand-binding sites (Extended Data Fig. 3b). We incorporated a polyethylene glycol unit of varying lengths and used the azide–alkyne cycloaddition reaction to synthesize RapaLink-1, -2 and -3 (Fig. 3b, Extended Data Fig. 3c and Supplementary Methods). Our modelling suggested that RapaLink-3, with an 11-heavy-atom linker would be too short to allow optimal binding to both sites simultaneously, while RapaLink-1 and -2, which contain 39- and 36-heavy-atom linkers, respectively, would allow simultaneous bivalent binding to the mTOR–FKBP12 complex.

Cells were treated with increasing concentrations of either RapaLink-1, -2 or -3, and the effects on mTOR signalling were assessed by western blotting. We observed that both RapaLink-1 and -2

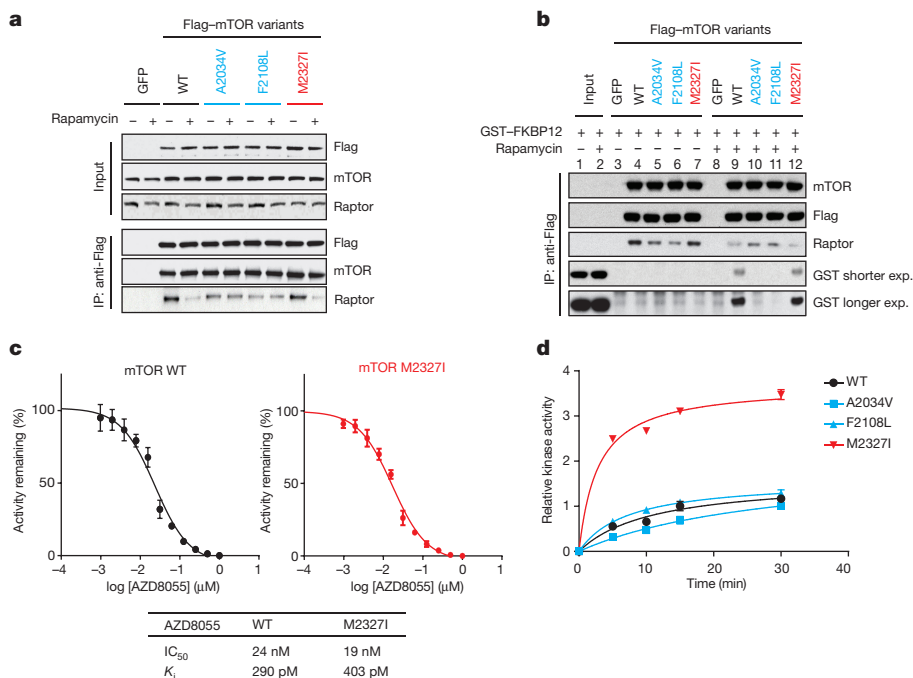


Figure 2 | Non-overlapping mechanisms of resistance mediated by mTOR mutations. **a**, mTOR-Flag wild-type (WT) and variants were transfected into 293H cells. Cells were treated with rapamycin and lysates were immunoprecipitated (IP) with an anti-Flag antibody. mTORC1 complex formation was assessed by immunoblotting. **b**, 293H cells were transfected and complex isolated as described in **a**, and an *in vitro* competition assay was performed followed by immunoblotting. Shorter and longer exposure (exp.) are shown. For gel source data, see Supplementary Fig. 2. **c**, Varying concentrations of AZD8055 were tested *in vitro* on wild-type and M2327I mTOR followed by a kinase reaction

inhibited the phosphorylation of both mTORC1 and mTORC2 targets at doses between 1 and 3 nM (Fig. 3c). However, RapaLink-3, which contains the shortest linker, showed diminished potency against the phosphorylation of 4EBP1 (T37/46/70 and S65) and AKT (S473) while still inhibiting p-S6 (S240/244 and S235/236). This is consistent with

(see Methods). The half-maximum inhibitory concentration (IC_{50}) values were determined by fitting to a standard four-parameter logistic using GraphPad Prism v.5. The diagram shows the mean of $n = 3$ data. The error bars represent the s.d. between experiments. **d**, 293H cells were transfected and the complex was isolated as described in **a**. An *in vitro* kinase assay was performed and the level of p-AKT (S473) was determined by immunoblotting. Symbols on each curve represent the relative p-AKT at different time points. The kinase activity curves were generated using GraphPad Prism v.6 after densitometry analysis was performed. All experiments were repeated at least three times.

the prediction that a longer linker is necessary to allow simultaneous binding to both drug sites and indicates that rapamycin binding is dominant over MLN0128 binding due to the preferential inhibition of p-S6 over p-4EBP1. Consistent with its strong signalling inhibition (Fig. 3d), RapaLink-1 potently inhibited the growth of MCF-7 cells at

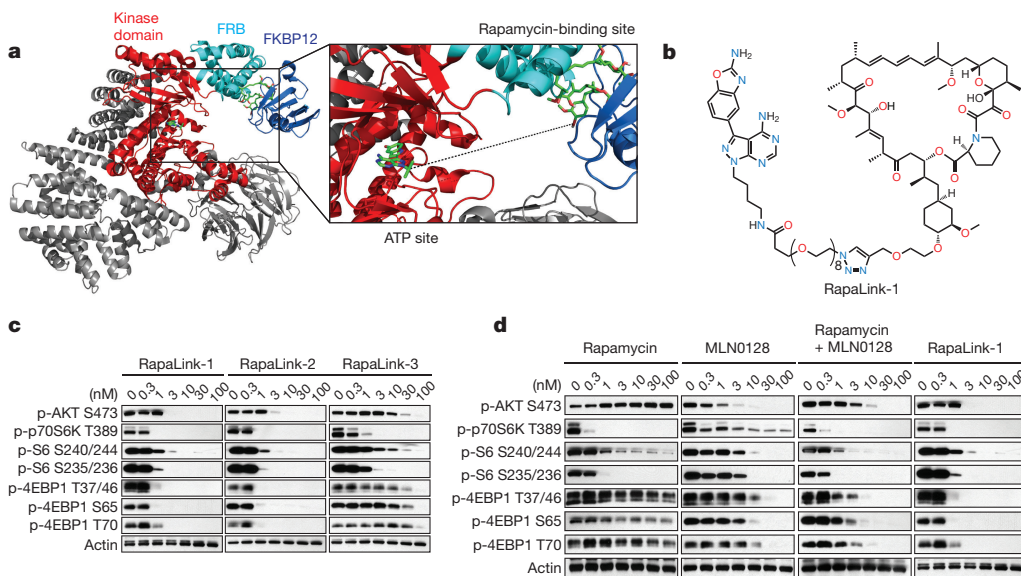


Figure 3 | RapaLink-1 is a potent mTOR inhibitor. **a**, Molecular model constructed by two available co-crystal structures, mTOR catalytic-domain-bearing TORKi PP242 (PDB, 4JT5) and mTOR FRB-domain-rapamycin-FKBP12 (PDB, 1FAP). Dotted line represents a guide line for the linker design of bivalent mTOR inhibitors. **b**, RapaLink-1 structure is displayed. **c**, **d**, MCF-7 cells were treated with RapaLink-1, -2 and -3 (**c**)

or with rapamycin, MLN0128, or a combination of rapamycin and MLN0128 or RapaLink-1 (**d**) for 4 h followed by immunoblotting. The rapamycin panel is the same as that shown in Fig. 1b and the RapaLink-1 panel is the same as that shown in **c**. All cellular experiments were repeated three times. For gel source data, see Supplementary Fig. 3.

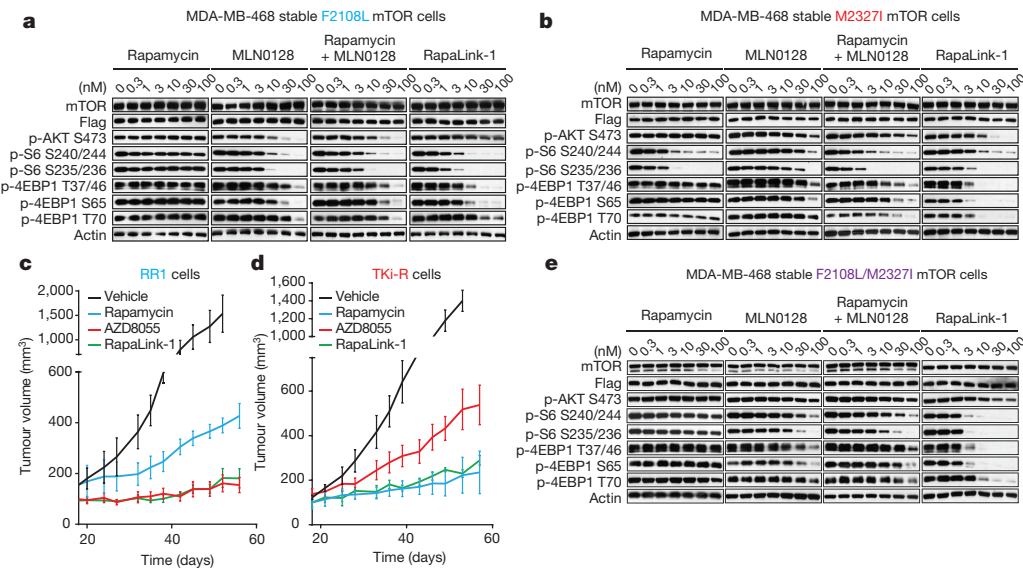


Figure 4 | RapaLink-1 reverses resistance due to mTOR FRB and kinase domain mutations. **a, b, e**, MDA-MB-468 cells inducibly expressing mTOR F2108L (**a**) or M2327I (**b**) or F2108L/M2327I mTOR double mutant (**e**) were treated as in Fig. 3d, followed by immunoblotting. For gel source data, see Supplementary Figs 4, 5 and 6. All experiments were repeated at least three times. **c, d**, Mice bearing RR1 (**c**) or TKi-R (**d**)

levels comparable to rapamycin or a combination of rapamycin with MLN0128 (Extended Data Figs 4a and 5).

We further tested the requirement of both halves of RapaLink-1 to simultaneously bind mTOR. First, we measured the ability of RapaLink-1 to recruit FKBP12 to mTOR by performing an *in vitro* FKBP12-binding assay; we show that RapaLink-1 is indeed able to recruit glutathione S-transferase (GST)-FKBP12 to wild-type mTOR (Extended Data Fig. 4b, lane 12). Moreover, we used the FKBP12 competitive ligand, FK506, to pharmacologically block RapaLink-1 from interacting with FKBP12 and thus mTOR. We observed that FK506 completely rescued the phosphorylation of mTORC1 and C2 substrates upon RapaLink-1 treatment (Extended Data Fig. 4c). Last, we isolated MCF-7 RapaLink-1-resistant cells; these cells harbour a mutation located in the mTOR FRB domain at position F2039S. As shown in Extended Data Fig. 6a, rapamycin treatment did not inhibit p-S6K (T389) and p-S6 (S240/244 and S235/236) in the mTOR F2039S cells as observed in the MCF-7 cells (Fig. 1b). Moreover, these cells displayed a decreased sensitivity to MLN0128 and a combination of rapamycin and MLN0128, as well as RapaLink-1 as compared to parental MCF-7 cells (Fig. 3d). Taken together, these data demonstrate that the binding of RapaLink-1–FKBP12 to the FRB domain is necessary for simultaneous binding to the ATP site of mTOR and therefore for RapaLink-1-dependent inhibition of mTOR signalling.

While the design of bivalent inhibitors for therapeutic use has had mixed success owing to the poor pharmaceutical properties of the hybrid molecules¹⁹, FKBP12-binding hybrids have actually been used to improve the pharmaceutical properties of small-molecule inhibitors unrelated to TORKi. These FK506-based hybrids exploit the high intracellular concentration of FKBP12, specifically in blood cells, and the high affinity of FK506 for FKBP12, to create a reservoir of drug that prolongs serum half-life²⁰. In agreement with the improved pharmaceutical properties of previous FKBP12-binding hybrids, RapaLink-1 showed prolonged inhibition of mTOR signalling *in vitro* (Extended Data Fig. 6b, c), as well as *in vivo* after a tolerable dose of 1.5 mg kg⁻¹, which lasted for over 4 days (Extended Data Fig. 6d, e) and was able to inhibit the growth of wild-type mTOR MCF-7 xenografts as well as the current clinical mTOR inhibitors (Extended Data Fig. 6f).

To assess whether RapaLink-1 could block mTOR signalling of the F2108L mTOR and M2327I mTOR drug-resistant mutants,

xenograft tumours ($n=5$ for each group) were randomized to four different groups: (1) vehicle (Monday (M), Wednesday (W), Friday (F)); (2) rapamycin (10 mg kg⁻¹; M, W, F); (3) AZD8055 (75 mg kg⁻¹; M, W, F); and (4) RapaLink-1 (1.5 mg kg⁻¹; weekly). Tumour size was measured by calliper twice per week. The results were reported as tumour volume (mm³) \pm s.d.

MDA-MB-468 cells expressing the alleles were treated with either rapamycin, MLN0128, a combination of both drugs, or RapaLink-1. Consistent with the ability of the RapaLink-1–FKBP12 complex to bind mTOR FRB and kinase-domain mutants (Extended Data Fig. 4b, lanes 18 and 24), and increased avidity compared to rapamycin or MLN0128 (Extended Data Fig. 7a); RapaLink-1 at low doses (3–10 nM) was the only drug regimen capable of inhibiting mTOR signalling in both F2108L mTOR- and M2327I mTOR-expressing cells (Fig. 4a, b). Mouse xenografts of MCF-7 cells expressing the RR1 mutant A2034V mTOR showed significantly less sensitivity to rapamycin yet maintained full sensitivity to AZD8055 and RapaLink-1 treatment (Extended Data Fig. 7b and Fig. 4c). Similarly, xenografts with MCF-7 cells expressing the TKi-R mutant, M2327I mTOR, showed significantly less sensitivity to AZD8055 treatment, yet retained full sensitivity to rapamycin and RapaLink-1 (Extended Data Fig. 7c and Fig. 4d). The dosing of RapaLink-1 may be limited by toxicity, which can only be tested in the clinic. However, our preclinical data and that of others²¹ indicate that mTOR kinase inhibitors can be given safely when administered intermittently and are more effective than daily dosing schedules.

It is reasonable to anticipate that patients bearing hyperactive MTOR kinase domain mutations, who originally respond to rapalogs, may eventually relapse owing to the emergence of a second FRB mutation, as previously observed⁵. To test whether RapaLink-1 would be an effective mTOR inhibitor in this case, MDA-MB-468 cells expressing F2108L/M2327I mTOR mutations were generated. As expected, mTOR substrates were resistant to rapamycin, MLN0128 and to a combination of both treatments in the F2108L/M2327I double-mutant cells. Yet, the signalling of these double-mutant cells remained as sensitive as the mTOR wild-type cells to RapaLink-1 treatment (Fig. 4e and Extended Data Fig. 7d).

Through exploitation of both the ATP- and the FRB-binding sites of mTOR, we have developed a new class of mTOR inhibitor that potently inhibits tumour growth and signalling in wild-type mTOR-expressing cells as well as in cells that have acquired resistance to rapalogs or ATP-competitive inhibitors, or both. Such inhibitors have been developed for G-protein-coupled receptors²² (termed bitopic ligands) but have not been exploited in protein kinase inhibitor design. Interestingly, the only other bitopic kinase inhibitor we are aware of is the natural

CDK2/cyclin-A inhibitor p27. The peptidic inhibitor spans the cyclin box and extends into the ATP site of CDK2, creating a high-affinity, highly specific inhibitor²³. Perhaps other allosteric sites near the ATP pocket on kinases could be similarly exploited, such as the PIF pocket²⁴, or it might even be possible to bridge two adjacent ATP pockets in kinase complexes such as KSR-MEK²⁵.

Online Content Methods, along with any additional Extended Data display items and Source Data, are available in the online version of the paper; references unique to these sections appear only in the online paper.

Received 29 October 2015; accepted 31 March 2016.

Published online 18 May 2016.

1. Vivanco, I. & Sawyers, C. L. The phosphatidylinositol 3-kinase AKT pathway in human cancer. *Nature Rev. Cancer* **2**, 489–501 (2002).
2. Basu, B. et al. First-in-human pharmacokinetic and pharmacodynamic study of the dual m-TORC 1/2 inhibitor AZD2014. *Clin. Cancer Res.* **21**, 3412–3419 (2015).
3. Iyer, G. et al. Genome sequencing identifies a basis for everolimus sensitivity. *Science* **338**, 221 (2012).
4. Wagle, N. et al. Activating mTOR mutations in a patient with an extraordinary response on a phase I trial of everolimus and pazopanib. *Cancer Discov.* **4**, 546–553 (2014).
5. Wagle, N. et al. Response and acquired resistance to everolimus in anaplastic thyroid cancer. *N. Engl. J. Med.* **371**, 1426–1433 (2014).
6. Feldman, M. E. et al. Active-site inhibitors of mTOR target rapamycin-resistant outputs of mTORC1 and mTORC2. *PLoS Biol.* **7**, e38 (2009).
7. Thoreen, C. C. et al. An ATP-competitive mammalian target of rapamycin inhibitor reveals rapamycin-resistant functions of mTORC1. *J. Biol. Chem.* **284**, 8023–8032 (2009).
8. Dowling, R. J. O. et al. mTORC1-mediated cell proliferation, but not cell growth, controlled by the 4E-BPs. *Science* **328**, 1172–1176 (2010).
9. Brown, E. J. et al. Control of p70 S6 kinase by kinase activity of FRAP *in vivo*. *Nature* **377**, 441–446 (1995).
10. Chen, J., Zheng, X. F., Brown, E. J. & Schreiber, S. L. Identification of an 11-kDa FKBP12-rapamycin-binding domain within the 289-kDa FKBP12-rapamycin-associated protein and characterization of a critical serine residue. *Proc. Natl. Acad. Sci. USA* **92**, 4947–4951 (1995).
11. Hara, K. et al. Regulation of eIF-4E BP1 phosphorylation by mTOR. *J. Biol. Chem.* **272**, 26457–26463 (1997).
12. Lorenz, M. C. & Heitman, J. TOR mutations confer rapamycin resistance by preventing interaction with FKBP12-rapamycin. *J. Biol. Chem.* **270**, 27531–27537 (1995).
13. Yang, H. et al. mTOR kinase structure, mechanism and regulation. *Nature* **497**, 217–223 (2013).
14. Grabiner, B. C. et al. A diverse array of cancer-associated MTOR mutations are hyperactivating and can predict rapamycin sensitivity. *Cancer Discov.* **4**, 554–563 (2014).
15. Cerami, E. et al. The cBio cancer genomics portal: an open platform for exploring multidimensional cancer genomics data. *Cancer Discov.* **2**, 401–404 (2012).
16. Mammen, M., Choi, S. K. & Whitesides, G. M. Polyvalent interactions in biological systems: Implications for design and use of multivalent ligands and inhibitors. *Angew. Chem. Int. Ed.* **37**, 2754–2794 (1998).
17. Hsieh, A. C. et al. The translational landscape of mTOR signalling steers cancer initiation and metastasis. *Nature* **485**, 55–61 (2012).
18. Molecular Operating Environment (Chemical Computing Group Inc., Montreal, Canada, 2016).
19. Szczepankiewicz, B. G. et al. Discovery of a potent, selective protein tyrosine phosphatase 1B inhibitor using a linked-fragment strategy. *J. Am. Chem. Soc.* **125**, 4087–4096 (2003).
20. Marinac, P. S. et al. FK506-binding protein (FKBP) partitions a modified HIV protease inhibitor into blood cells and prolongs its lifetime *in vivo*. *Proc. Natl. Acad. Sci. USA* **106**, 1336–1341 (2009).
21. Patel, M. R. et al. A phase I study evaluating continuous and intermittent AZD2014 in combination with fulvestrant in patients with ER⁺ advanced metastatic breast cancer (abstract). *Proc. AACR 106th Ann. Meeting* CT233.25 (AACR, 2015).
22. Valant, C., Robert Lane, J., Sexton, P. M. & Christopoulos, A. The best of both worlds? Bitopic orthosteric/allosteric ligands of G protein-coupled receptors. *Annu. Rev. Pharmacol. Toxicol.* **52**, 153–178 (2012).
23. Russo, A. A., Jeffrey, P. D., Patten, A. K., Massagué, J. & Pavletich, N. P. Crystal structure of the p27^{Kip1} cyclin-dependent-kinase inhibitor bound to the cyclin A-Cdk2 complex. *Nature* **382**, 325–331 (1996).
24. Wei, L. et al. Design and synthesis of benzoazepin-2-one analogs as allosteric binders targeting the PIF pocket of PDK1. *Bioorg. Med. Chem. Lett.* **20**, 3897–3902 (2010).
25. Brennan, D. F. et al. A Raf-induced allosteric transition of KSR stimulates phosphorylation of MEK. *Nature* **472**, 366–369 (2011).

Supplementary Information is available in the online version of the paper.

Acknowledgements N.R. would like to thank the National Institutes of Health (NIH) (P01 CA094060) for funding, as well as the Breast Cancer Research Foundation grant and the National Cancer Institute Cancer Center Support grant P30 CA008748, W. H. Goodwin and A. Goodwin, the Commonwealth Foundation for Cancer Research, The Center for Experimental Therapeutics at Memorial Sloan Kettering Cancer Center, and the team up for a Cure Fund. K.M.S. would like to thank the NIH P50 AA017072, the Stand Up 2 Cancer Lung Cancer Dream Team, The Samuel Waxman Cancer Research Foundation and the Howard Hughes Medical Institute for funding. We would like to thank R. Mukherjee, S. Schwartz, J. Taunton and B. Roth for helpful comments.

Author Contributions V.S.R.-O., M.O., Z.Y., C.J.N., N.R. and K.M.S. conceived the project, designed and analysed the experiments, and wrote the manuscript. V.S.R.-O., M.O., Z.Y., C.J.N., C.M., A.B., W.W., D.G.B., S.C. and T.K. performed and supervised the laboratory experiments. H.W. and M.B. performed and supervised the IMPACT sequencing and analysis. E.d.S. designed and supervised the *in vivo* experiments.

Author Information Reprints and permissions information is available at www.nature.com/reprints. The authors declare competing financial interests: details are available in the online version of the paper. Readers are welcome to comment on the online version of the paper. Correspondence and requests for materials should be addressed to K.M.S. (kevan.shokat@ucsf.edu) or N.R. (roenn@mskcc.org).

METHODS

Cell culture and reagents. All cell lines were obtained from the American Type Culture Collection (ATCC). MCF-7 and MDA-MB-468 (ATCC catalogue numbers HTB-22 and HTB-132, respectively) breast cancer cell lines were maintained in a 1:1 mixture of DMEM:F12 medium supplemented with 4 mM glutamine, 100 units ml⁻¹ each of penicillin and streptomycin, and 10% heat-inactivated fetal bovine serum (FBS) and incubated at 37 °C in 5% CO₂. The MDA-MB-468 inducible expression cells were maintained in the same medium with addition of 50 µg ml⁻¹ hygromycin and 0.2 µg ml⁻¹ puromycin. The HEK-293 cells (ATCC catalogue number CRL-1573) were maintained in DMEM medium with glutamine, antibiotics and 10% FBS. The cell lines tested negative for mycoplasma contamination. AZD8055 was obtained from AstraZeneca Pharmaceuticals, rapamycin was purchased from EMD Bioscience. RAD001, KU006, WY354, PP242 and MLN0128 were purchased from Tocris. Doxycycline was purchased from Sigma-Aldrich. Puromycin and hygromycin stock solution were purchased from Invitrogen. Drugs were dissolved in DMSO to yield 10 mM stock and stored at -20 °C.

Selection of drug-resistant clones. Cell lines resistant to rapamycin (RR1 and RR2) and AZD8055 (TKI-R) were generated by exposing the parental breast cancer cell line MCF-7 to a high dose of drug (500 nM of either rapamycin or AZD8055) for 3 months of continuous drug exposure (change of media every 3 days); the cells were then sent to sequencing. MCF-7-RapaLink-1-resistant cells were generated by exposing MCF-7 cells to RapaLink-1 (10 nM) for 9 months of continuous drug exposure (change of media once per week); the cells were then sent to sequencing. **Genomic DNA sequencing.** We profiled genomic alterations in 279 key cancer-associated genes using our integrated mutation profiling of actionable cancer targets (IMPACT) assay, which utilizes solution-phase hybridization-based exon capture and massively parallel DNA sequencing. Custom oligonucleotides were designed to capture all protein-coding exons and select introns of 279 commonly implicated oncogenes, tumour suppressor genes, and members of pathways deemed actionable by targeted therapies. We prepared barcoded sequence libraries (New England Biolabs, Kapa Biosystems) for DNA from the MCF-7 parental cell line and drug-resistant subclones, and we performed exon capture on barcoded pools by hybridization (Nimblegen SeqCap). Two-hundred and fifty nanograms of genomic DNA was input for library construction. Libraries were pooled at equimolar concentrations (100 ng per library), combined with barcoded libraries from a separate project, and input to a single exon capture reaction as previously described²⁶. DNA was subsequently sequenced on an Illumina HiSeq 2000 to generate paired-end 75-bp reads. We achieved a mean unique sequence coverage of 487 × per sample.

Method for construction of docking modelling. The coordinate of the crystal structure of rapamycin with FKBP12 and the FRB domain was retrieved from the PDB (accession 1FAP). The coordinate of the crystal structure of ATP-competitive mTOR inhibitor (PP242) with mTORΔN and mLST8 was retrieved from the PDB (accession 4J5). Two co-crystal structures were aligned and amino acids and water molecules in the FRB domain of 1FAP were deleted. The coordinate of co-crystal structure unavailable ATP-competitive mTOR inhibitor (MLN0128) was manually constructed by modifying the coordinate of the co-crystal structure of its analogue (PP242). The obtained modelling containing rapamycin and MLN0128 was energy-minimized using the MMFF94x force field in Molecular Operating Environment (MOE; described later)¹⁸ to provide a template structure. During the minimization procedure, the following conditions were adopted. The dielectric constant was set to 4 × *r*, where *r* is the interatomic distance. The residues, which are 9 Å away from compound, were fixed. And atomic charges for the protein and the compounds were set according to the AMBER99 and the AM1-BCC method, respectively. A crosslinker tethering rapamycin with an ATP-competitive mTOR inhibitor was manually constructed and energy-minimized using the MMFF94x force field in MOE to provide the initial conformation. The obtained initial conformation was subjected to conformation search using LowModeMD in MOE (iterative limitation was set as 30). Values of potential energies (kcal mol⁻¹) of automatically created conformation(s) were averaged.

Code availability. MOE (version 2013.0801, Chemical Computing Group, Montreal, Canada), Scientific Vector Language (SVL) source.

Cell proliferation assay. The effect of the drug on cell proliferation was determined using a CellTiter-Glo Luminescent Cell Viability Assay kit (Promega), which is based on quantification of the cellular ATP level. Cells were plated in 96-well plates at a density of 2,000–5,000 cells (8 replicates per condition). The following day, cells were treated with a range of drug concentrations prepared by serial dilution. After 1–3 days of treatment, 100 µl of prepared reagent was added to each well. The contents of the wells were mixed on a plate shaker for 1 h, and then luminescence was measured by an Analyst AD (Molecular Devices). The relative growth was normalized to the untreated samples in each group. The growth or inhibition curves and IC₅₀ values were calculated with Graph Pad Prism v.6.

Immunoblot analysis. Cells were washed with PBS once, disrupted on ice for 30 min in NP-40 (50 mM Tris (pH 7.4), 1% NP-40, 150 mM NaCl, 40 mM NaF) or RIPA lysis buffer (Thermo Scientific) supplemented with protease and phosphatase inhibitors (Pierce Chemical) and cleared by centrifugation. Protein concentration was determined with BCA reagent from Pierce. Equal amounts of protein (10 to 50 µg) in cell lysates were separated by SDS-PAGE, transferred to nitrocellulose membranes (GE healthcare), immunoblotted with specific primary and secondary antibodies and detected by chemiluminescence with the ECL detection reagents from Amersham Biosciences. Antibodies for p-AKT (S473) (#4060L), p-p70S6K (T389) (#9234L), p-S6 (S240/244) (#5364L) and p-S6 (S235/236) (#4858L), p-4EBP1 (T37/46) (#9459L), p-4EBP1 (S65) (#9451L), p-4EBP1 (T70) (#9455L), β-actin (#4970S), mTOR (#2972S) and raptor (#2280S) were purchased from Cell Signaling Technology. The Flag (#F1804) antibody was purchased from Sigma. The GST antibody (#sc-138) was from Santa Cruz.

Retrovirus-based gene-inducible expression cell system. The mTOR genes were sub-cloned into TTIGFP-MLUEX vector harbouring tet-regulated promoter. Mutations were introduced by using the site-directed Mutagenesis Kit (Stratagene) as previously described²⁷. The retroviruses encoding the rtTA3 or MTOR genes were packaged in Phoenix-AMPHO cells. The medium containing virus was filtered with 0.45 PVDF filters followed by incubation with the target cells for 6 h. The cells were then cultured in virus-free medium for 2 days. The cells were selected with puromycin (2 µg ml⁻¹) or hygromycin (500 µg ml⁻¹) for 3 days. The positive infected cell populations were further sorted with transiently expressed GFP marker after being exposed to 1 µg ml⁻¹ doxycycline and the sorted positive cells were cultured and expanded in medium without doxycycline but with antibiotics at a maintaining dose until the following assays.

Transient transfections. Cells were seeded at 60-mm or 100-mm plates and transfected the following day using Lipofectamine 2000 (Invitrogen) according to the manufacturer's instructions. The ratio between DNA and lipofectamine was 1 µg DNA to 3 µl lipofectamine.

In vitro FKBP12 binding assay. Cells expressing Flag-tagged wild-type or mutant mTOR were collected and lysed with 0.3% CHAPS buffer. The mTOR complexes were pulled down with anti-Flag antibody-conjugated agarose. Then, the bead-bound complexes were incubated with recombinant FKBP12 (Fisher Scientific) (250 nM) or FKBP12 (250 nM) and rapamycin (250 nM) at 4 °C for 30 min. After incubation, the beads were washed five times with CHAPS buffer. The protein complexes were eluted with 1 × Laemmli Buffer and assayed by western blotting.

Sequencing Sanger. The complementary DNA was generated by messenger RNA isolated from cell pellets with SV total RNA isolation kit, SV minipreps DNA purification kit and ImProm-II Reverse Transcription System kit from Promega. The mTOR cDNA was amplified with the oligonucleotides listed in Supplementary Methods. The PCR products were subjected to gel purification and sequenced by Genewiz.

Mutagenesis. All the mTOR mutants were generated by QuikChange II Site-Directed Mutagenesis Kit obtained from Agilent and confirmed by Sanger sequencing.

mTOR *in vitro* kinase assay. Active mTOR kinases were expressed in 293 cells and isolated by immunoprecipitation with anti-Flag beads in 0.3% CHAPS buffer. The AKT recombinant protein was acquired from AstraZeneca Pharmaceuticals. The *in vitro* kinase assays was performed with 250 µM ATP at 37 °C for 20 min.

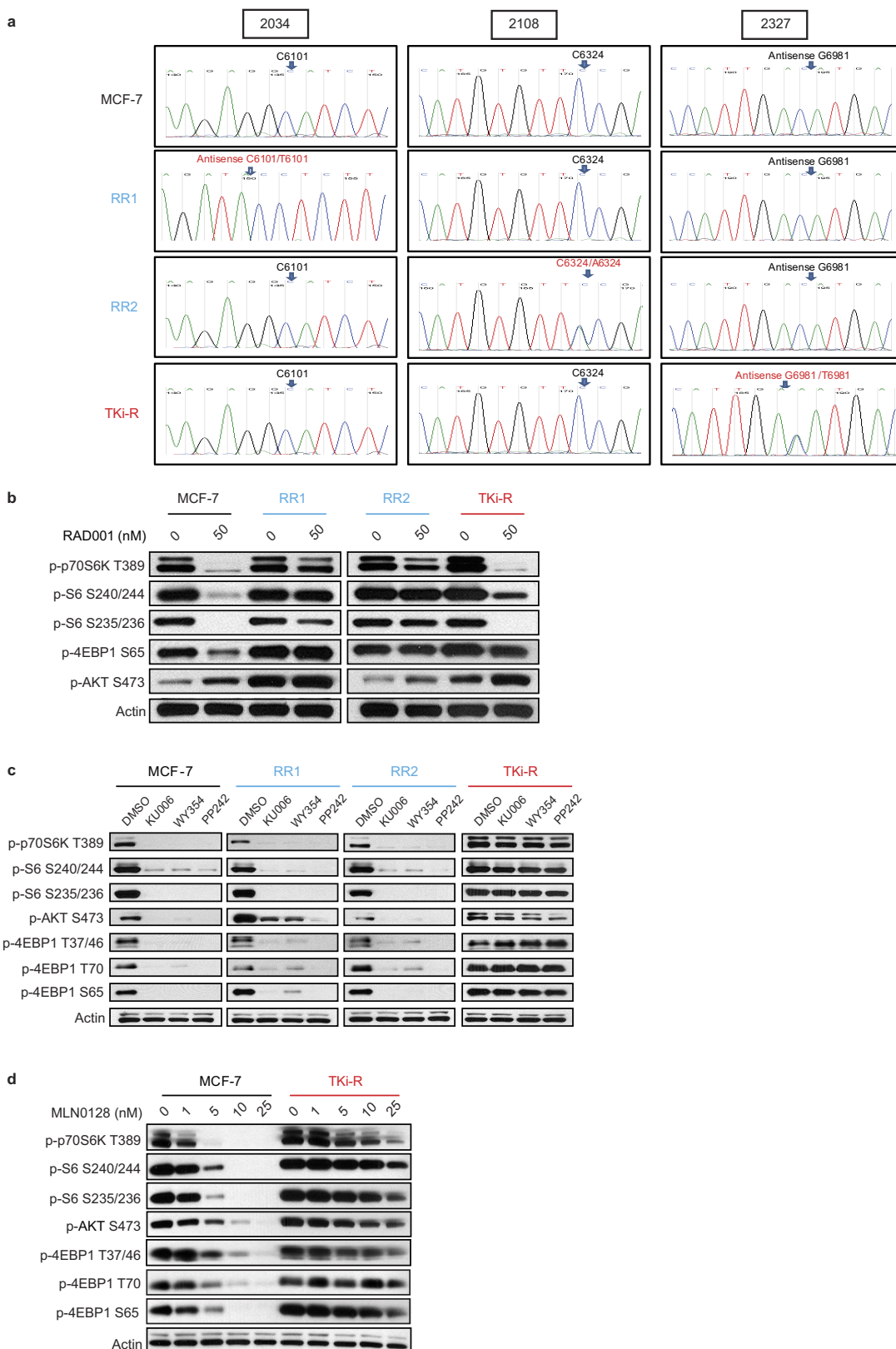
In vitro kinase inhibition assay. Concentration-response curves with a concentration range of 1,000 to 0.97 nM and twofold serial dilution were constructed by dispensing a 100 µM DMSO solubilized stock of AZD8055 into white 384-well medium-binding microplates (Greiner Bio-One) using an HP D3000 Digital Dispenser. The kinase reaction was performed as described earlier using 200 µM ATP, 1.5 µM peptide substrate and either 5 nM wild-type mTOR or 2 nM M2327I mutant mTOR. The IC₅₀ values were calculated from initial rate data before being corrected for competition with ATP using the Cheng-Prusoff equation and assuming the compound is fully ATP competitive²⁸. The IC₅₀ values were determined by fitting to a standard four-parameter logistic using GraphPad Prism v.5.

Animal studies. All *in vivo* studies were conducted in accordance with guidelines approved by the Memorial Sloan-Kettering Cancer Center (MSKCC) Institutional Animal Care and Use Committee (IACUC). The maximal tumour volume permitted by the MSKCC IACUC is 2,000 mm³; this limit was not exceeded in any of the experiments. Eight-week-old athymic nu/nu female mice (Harlan Laboratories) were injected subcutaneously with 10 million cells together with matrigel (BD Biosciences). 17β-Oestradiol pellets (0.72 mg/90 days release) (Innovative Research of America) were implanted subcutaneously 3 days before tumour cell inoculation. Once tumours reached an average volume of 100 mm³, mice were randomized (*n* = 5 mice per group) to receive rapamycin (10 mg kg⁻¹), AZD8055 (75 mg kg⁻¹), RapaLink-1 (1.5 mg kg⁻¹) or vehicle only as control. Sample size was chosen based on previous experiments. Rapamycin was formulated in DMSO and delivered

intraperitoneally, AZD8055 was formulated in 30% captisol, and administered orally, RapaLink-1 was formulated in 6% DMSO and 30% captisol and delivered intraperitoneally. Mice treated with RapaLink-1 were also given subcutaneous saline injections twice a day, along with water supplemented with 5% glucose. Tumours were measured twice weekly using callipers, and tumour volume was calculated using the formula: length \times width² \times 0.52. Samples were lysed and processed as previously described²⁹.

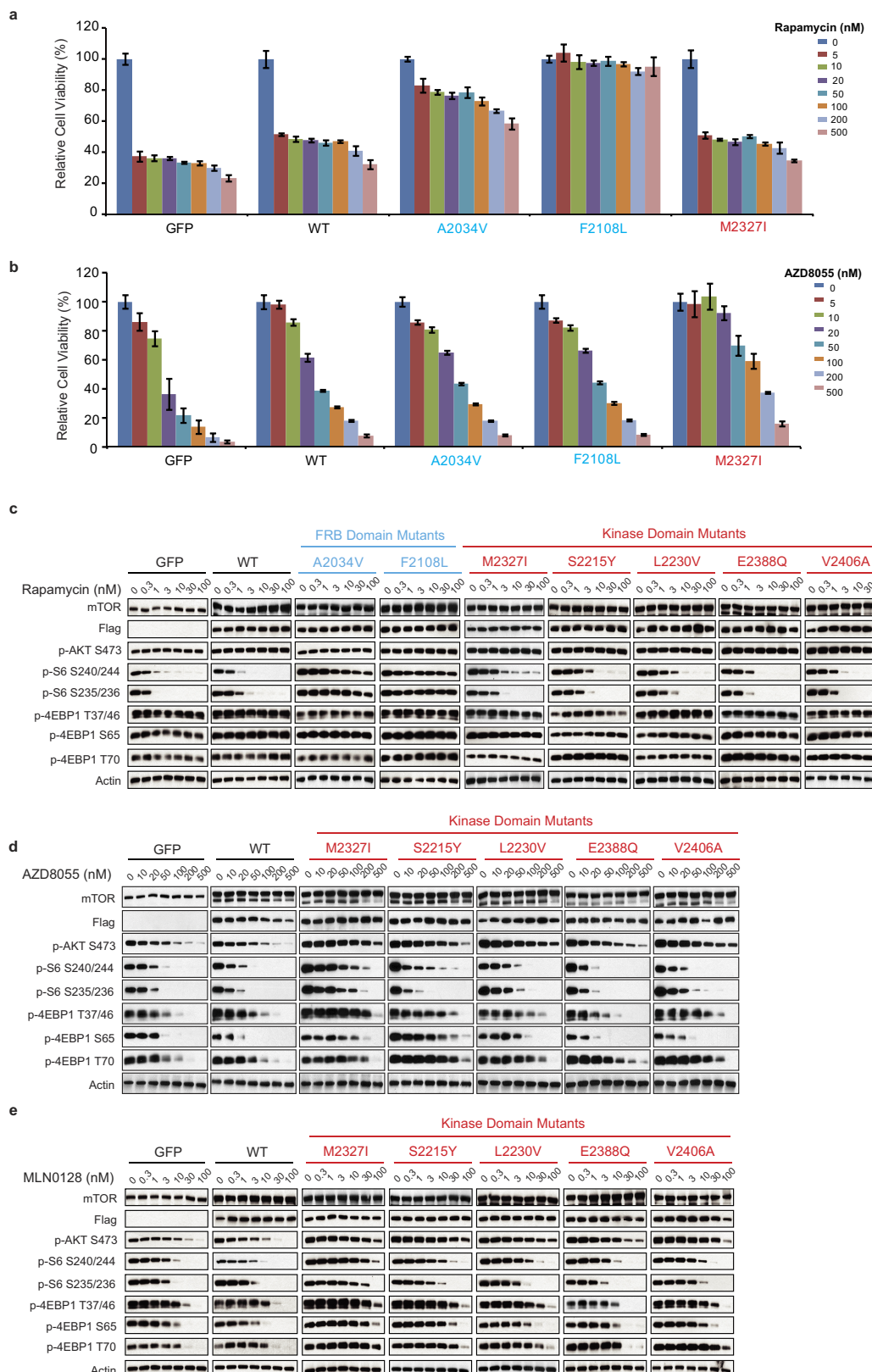
Statistical analysis. Results are mean values \pm s.d. Investigators were not blinded when assessing the outcome of the *in vivo* experiments. All cellular experiments were repeated at least three times.

26. Juric, D. *et al.* Convergent loss of PTEN leads to clinical resistance to a PI(3)K α inhibitor. *Nature* **518**, 240–244 (2015).
27. Yao, Z. *et al.* BRAF mutants evade ERK-dependent feedback by different mechanisms that determine their sensitivity to pharmacologic inhibition. *Cancer Cell* **28**, 370–383 (2015).
28. Cheng, A. C., Eksterowicz, J., Geuns-Meyer, S. & Sun, Y. Analysis of kinase inhibitor selectivity using a thermodynamics-based partition index. *J. Med. Chem.* **53**, 4502–4510 (2010).
29. Rodrik-Outmezguine, V. S. *et al.* mTOR kinase inhibition causes feedback-dependent biphasic regulation of AKT signaling. *Cancer Discov.* **1**, 248–259 (2011).



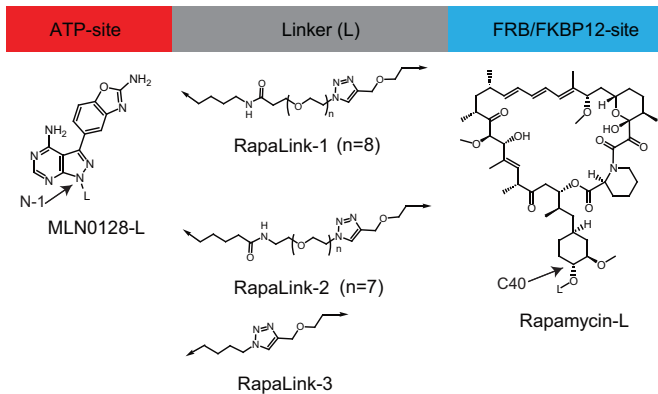
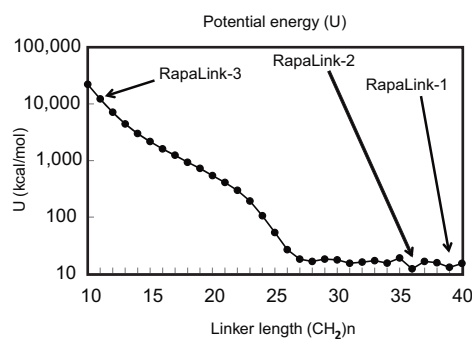
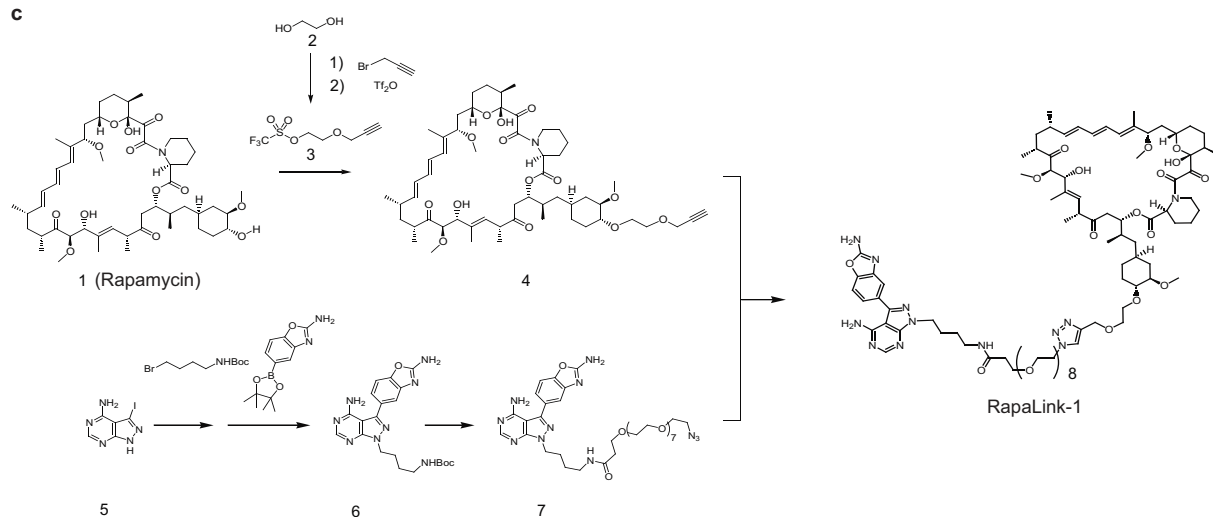
Extended Data Figure 1 | Acquired-mTOR mutations promote resistance to mTOR inhibitors in MCF-7 cells. **a**, The RNA from MCF-7 parental, RR1, RR2 and TKi-R cells was isolated and the polymerase chain reaction with reverse transcription (RT-PCR) products were submitted to Sanger sequencing at Genewiz. **b**, MCF-7 parental, RR1, RR2 and TKi-R cells were treated with either dimethylsulfoxide (DMSO) or 50 nM

of RAD001 for 4 h. Immunoblot analyses were performed on mTOR effectors. **c**, **d**, MCF-7 parental, RR1, RR2 and TKi-R cells were treated with either DMSO as a control or 500 nM of either KU006, WY354 or PP242 mTOR inhibitors (**c**), or with different doses of MLN0128 (**d**) for 4 h. Immunoblot analyses were performed on mTOR effectors. All cellular experiments were repeated at least three times.



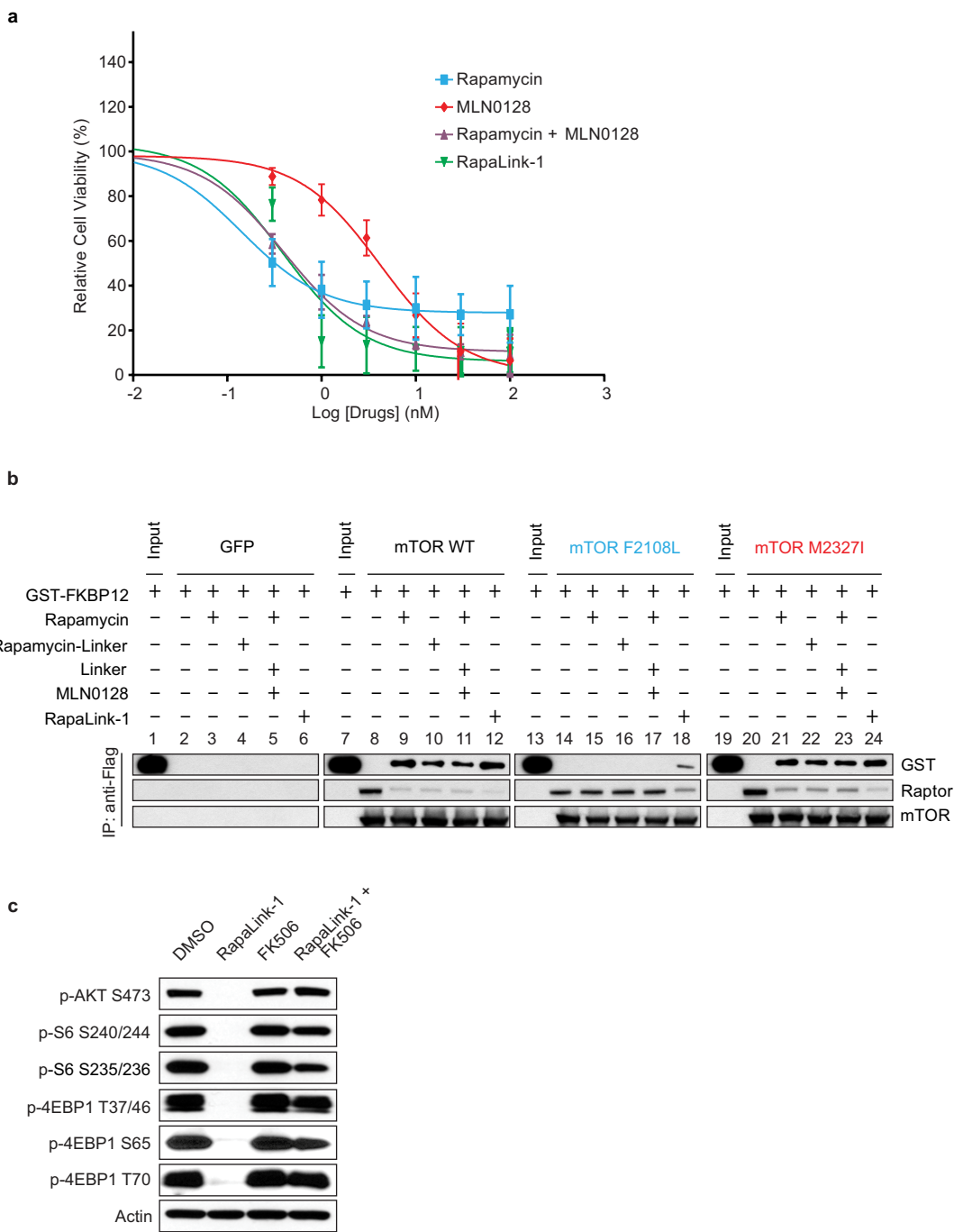
Extended Data Figure 2 | Acquired-mTOR mutations promote resistance to mTOR inhibitors in MDA-MB-468 cells. **a, b,** Dose-dependent cell growth inhibition of the MDA-MB-468 cells expressing green fluorescent protein (GFP), wild-type mTOR or different mTOR variants (A2034V, F2108L and M2327I) upon rapamycin (**a**) or AZD8055 treatment (**b**). Cells were pre-treated for 24 h with doxycycline (1 µg ml⁻¹)

to induce the expression of exogenous mTOR. The cell growth was determined as described in Fig. 1d. **c–e**, MDA-MB-468 cells expressing GFP, wild-type mTOR or different mTOR variants were treated with different concentrations of rapamycin (**c**), AZD8055 (**d**) or MLN0128 (**e**) for 4 h. Immunoblot analyses were performed on mTOR effectors. All cellular experiments were repeated at least three times.

a**b****c**

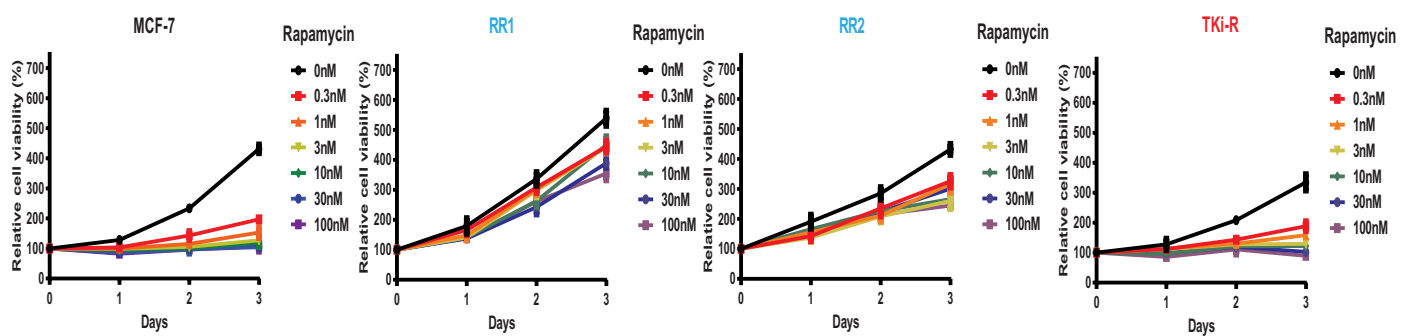
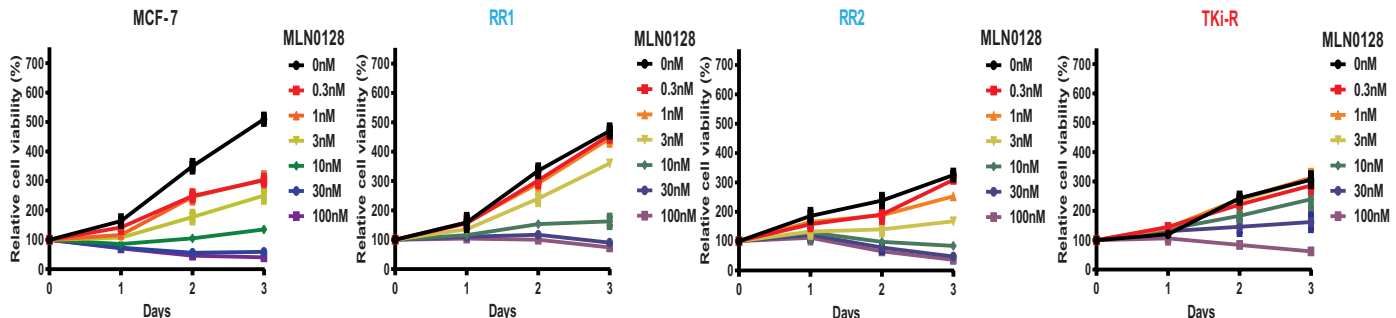
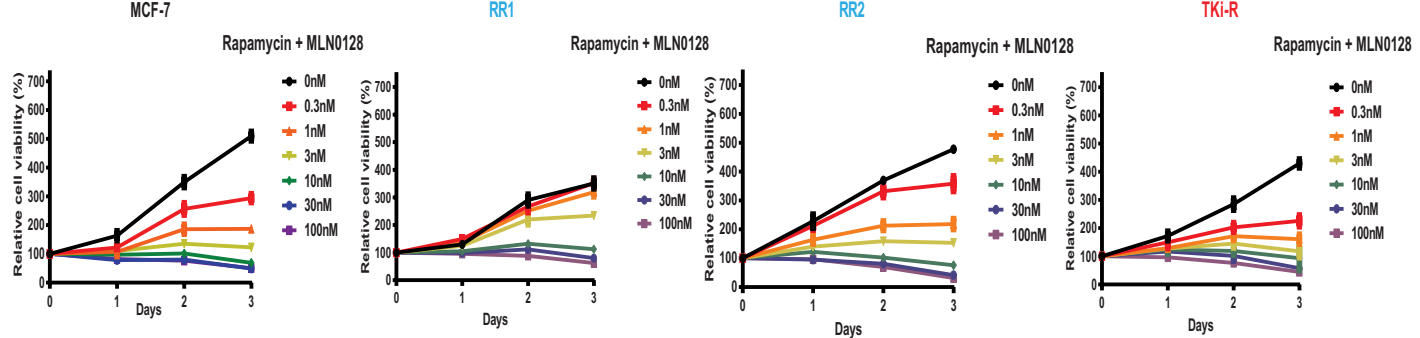
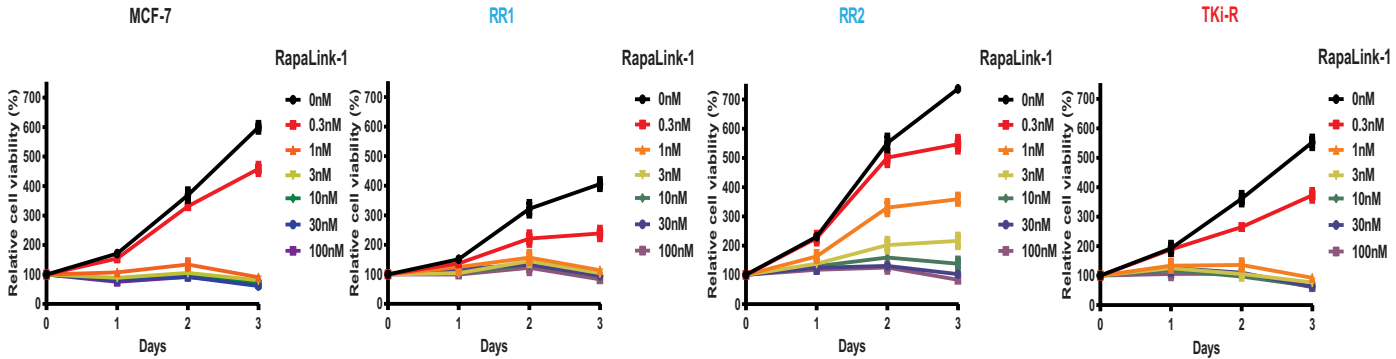
Extended Data Figure 3 | Synthesis of the mTOR bivalent inhibitor RapaLink-1. **a**, Compound design of RapaLink-1, -2, and -3 possessing a polyethylene glycol unit of varying lengths. **b**, Calculated potential energy units (U) (kcal mol^{-1}) of modelled compounds of varying methylene

(CH_2n) linker lengths for bivalent interactions with the catalytic site and the FKBP12 site. **c**, A convergent synthetic route for a bivalent mTOR inhibitor RapaLink-1.

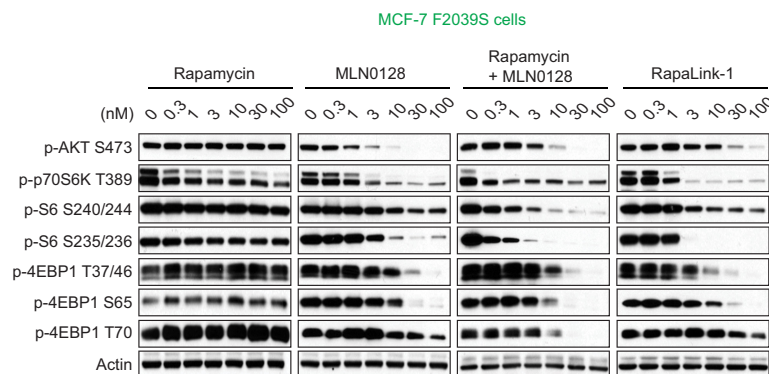
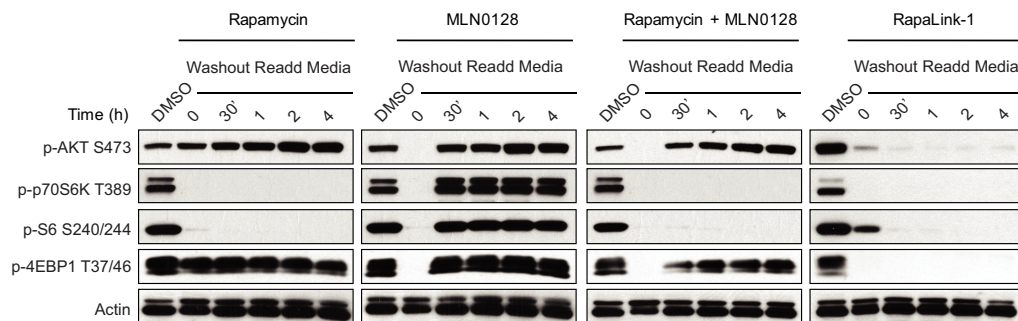
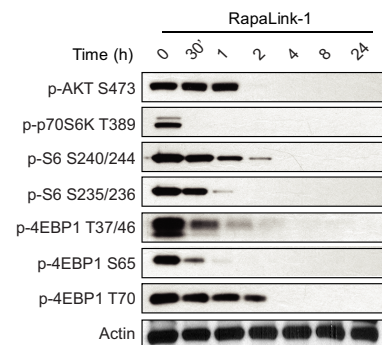
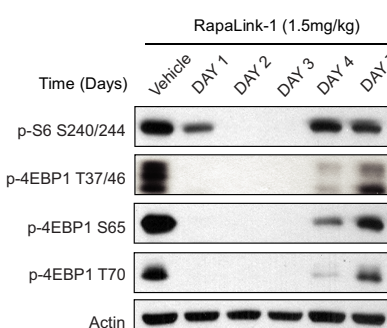
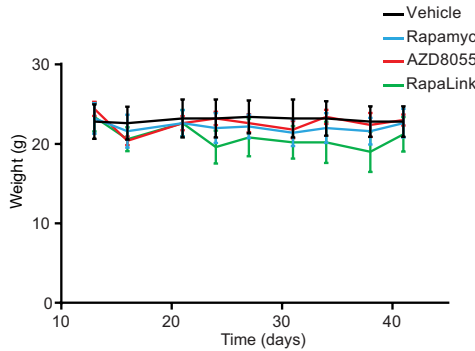
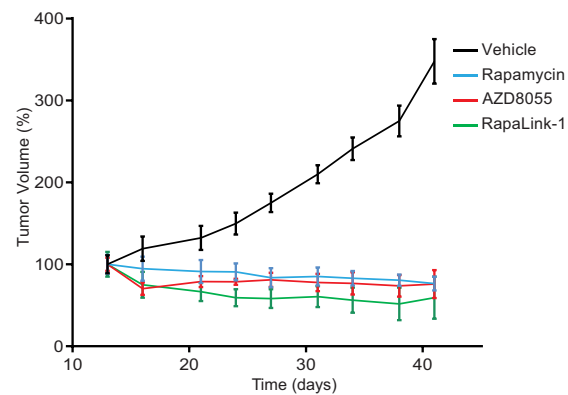


Extended Data Figure 4 | RapaLink-1 requires FKBP12 for binding to the mTOR FRB domain. **a**, Dose-dependent cell growth inhibition curves of the MCF-7 parental cell line treated with rapamycin, MLN0128, a combination of rapamycin and MLN0128, or RapaLink-1. The cell growth was determined as described in Fig. 1d. **b**, mTOR-Flag wild type and variants were transfected into 293H cells. The mTORC1 complex was

isolated, and an *in vitro* competition assay in the presence of FKBP12 was performed as described in Fig. 2b. **c**, MCF-7 cells were treated with either DMSO, RapaLink-1 (10 nM), FK506 (10 μ M), or a combination of both for 24 h, at which time the cells were collected. Immunoblot analyses were performed on mTOR signalling. All experiments were repeated at least three times.

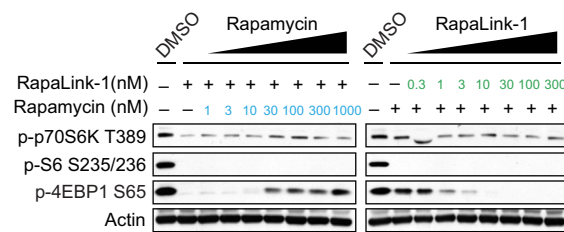
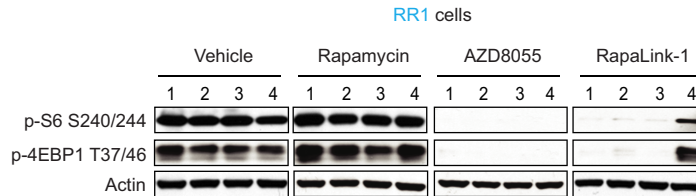
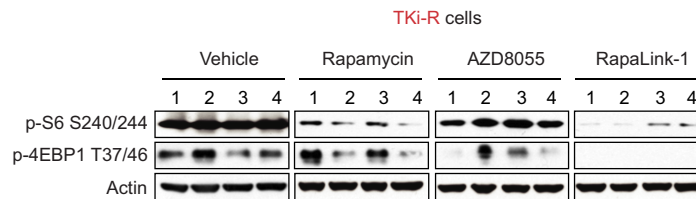
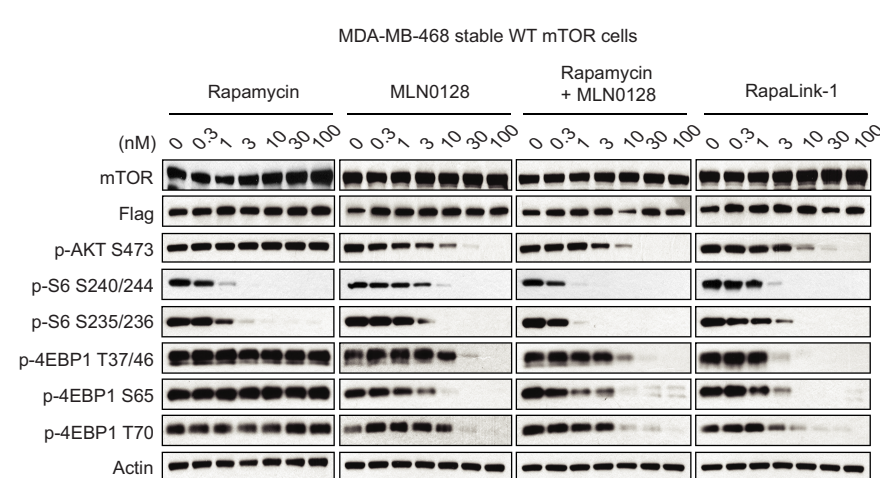
a**b****c****d**

Extended Data Figure 5 | RapaLink-1 is a potent mTOR inhibitor in wild-type and mutant mTOR cells. **a–d**, MCF-7, RR1, RR2 and TKi-R cells were treated with different concentrations of rapamycin (**a**), MLN0128 (**b**), combination treatment (**c**) or RapaLink-1 (**d**) over 3 days. The cell growth was determined as described in Fig. 1d. Each dot and error bar on the curves represents mean \pm s.d. ($n=8$).

a**b****c****d****e****f**

Extended Data Figure 6 | RapaLink-1 has a prolonged intracellular half-life in wild-type mTOR cells. **a**, MCF-7 F2039S cells were treated with different concentrations of rapamycin, MLN0128, combination treatment or RapaLink-1 for 4 h, at which time the cells were collected. Immunoblot analyses were performed on mTOR signalling. **b**, MCF-7 cells were treated for 4 h with either DMSO control, 30 nM of rapamycin, 30 nM of MLN0128, a combination of 30 nM of both or 30 nM of RapaLink-1 for 4 h, at which time the treatments were washed out three times with PBS and fresh media was re-added for the indicated times. Immunoblot analyses were performed on mTOR effectors. **c**, MCF-7 cells were

treated with 10 nM of RapaLink-1 and collected at the indicated times. Immunoblot analyses were performed as described earlier. All experiments were repeated at least three times. **d**, Mice bearing MCF-7 xenograft tumours were treated with one single dose of vehicle or RapaLink-1 (1.5 mg kg^{-1}), tumours were collected at different days after treatment as indicated. Immunoblot analyses were performed on mTOR effectors. **e**, The weight of the mice treated in the efficacy study shown in **f** is reported here. **f**, Mice bearing MCF-7 xenograft tumours were treated as described in Fig. 4c ($n = 5$ for each group). The results were reported as percentage tumour volume \pm s.d.

a**b****c****d**

Extended Data Figure 7 | RapaLink-1 is a more potent mTOR inhibitor than rapamycin. **a**, MCF-7 cells were treated for 4 h with either RapaLink-1 (10 nM) or rapamycin (10 nM) with simultaneous addition of increasing doses of either rapamycin (left) or RapaLink-1 (right). Immunoblot analyses were performed on mTOR effectors. **b, c**, Mice bearing RR1 (b) or TKi-R (c) xenograft tumours were treated for 24 h with a single dose of either vehicle, rapamycin (10 mg kg⁻¹), AZD8055 (75 mg kg⁻¹)

or RapaLink-1 (1.5 mg kg⁻¹) ($n = 4$ for each group). Immunoblot analyses were performed on mTOR effectors. **d**, MDA-MB-468 cells inducibly expressing mTOR wild type were treated with either rapamycin, MLN0128, a combination of rapamycin and MLN0128, or RapaLink-1 for 4 h. Immunoblot analyses were performed on mTOR effectors with the indicated antibodies. Rapamycin and MLN0128 panels are the same shown for wild type in Extended Data Fig. 2c and e, respectively.

Extended Data Table 1 | mTOR mutations found in human patient samples

References	Histology	mTOR mutations	Domains	Treatments
TCGA-B0-4852-01	ccRCC (TCGA)	E2033V	FRB	Baseline
Wagle et al. 2014	Thyroid	F2108L	FRB	Everolimus
TCGA-DU-6393-01	Gloma (TCGA)	M2327I	Kinase	Baseline
TCGA-A3-3347-01	ccRCC (TCGA)	M2327I	Kinase	Baseline
P-00006559-T01-IM5	Colorectal Cancer (MSKCC-IMPACT)	M2327I	Kinase	Baseline
P-0000645-T01-IM3	Bladder Urothelial Carcinoma (MSKCC-IMPACT)	M2327I	Kinase	Baseline
ccRCC_28	ccRCC (U Tokyo)	M2327I	Kinase	Baseline
P-0000614-T01-IM3	Endometrial Cancer (MSKCC-IMPACT)	M2327V	Kinase	Baseline

List of some FRB and kinase domain mTOR mutations found in human patient samples. Data were collected from the cBioPortal, Memorial Sloan-Kettering Cancer Center (MSKCC).

Extended Data Table 2 | List of FRB domain mutations found in human patient samples

References	Cancer Study	Mutations
P-0004920-T01IM5	MSK-IMPACT	E2014K
SNU738_CENTRAL	CCLE	L2016R
BL41_HAEATOPOIE...	CCLE	I2017T
TCGA-KM-844101	chRCC (TCGA)	I2017T
P-0003073-T01IM5	MSK-IMPACT	I2017S
TCGA-66-2787-01	Lung squ (TCGA)	W2023G
BCP1_HAEMATOPOIE...	CCLE	G2030V
TCGA-B0-4852-01	ccRCC (TCGA)	E2033V
TCGA-B5-A1E-01	Uterine (TCGA)	A2056V
TCGA-G3-A25U-01	Liver (TCGA)	M2057I
TCGA-AZ-6598-01	Colorectal (TCGA)	Q2063fs
H072999	Liver (AMC)	K2066R
NCIH1792_LUNG	CCLE	Q2072
P-0000112-T01IM3	MSK-IMPACT	Q2072R
S05-31806-TP-NT	CSCC (Dana-Farber)	X2073_splice
P-0005266-T01IM5	MSK-IMPACT	R2076L
TCGA-EE-A2GC-06	Melanoma (TCGA)	D2077E
P-0002050-T01IM3	MSK-IMPACT	W2084C
TCGA-AX-A0J0	Uterine (TCGA)	Y2088D
TCGA-CQ-5327	Head & neck (TCGA)	M2089I
P-0005159-T01IM5	MSK-IMPACT	L2097F
TCGA-D8-A1Y0-01	Breast (TCGA)	W2101L

Data were collected from the cBioPortal, MSKCC.

Extended Data Table 3 | List of mTOR kinase domain mutations found in human patient samples

References	Cancer Study	Mutations
TCGA-C5-A1BM-01	Cervical (TCGA)	D2191H
TCGA-BR-4370-01	Stomach (TCGA)	R2193C
P-0004376-T01-IM5	MSK-IMPACT	F2202L
TCGA-BT-A0YX-01	Bladder (TCGA)	L2209V
TCGA-B0-4810-01	ccRCC (TCGA)	A2210P
JHUEM7-ENDOMETRIUM	CCLE	S2215Y
TCGA-JW-A5VL-01	Cervical (TCGA)	S2215Y
TCGA-FU-A3HZ-01	Cervical (TCGA)	S2215Y
TCGA-AA-A00K-01	Colorectal (TCGA)	S2215Y
TCGA-A6-6141-01	Colorectal (TCGA)	S2215Y
TCGA-F4-6806-01	Colorectal (TCGA)	S2215F
TCGA-DM-A1D4	Colorectal (TCGA)	S2215F
S12-23181-TP-NT	CSCC (Dana-Farber)	S2215F
TCGA-CJ-5679-01	ccRCC (TCGA)	S2215Y
TCGA-A4-7828-01	pRCC (TCGA)	S2215Y
P-0000208-T01-IM3	MSK-IMPACT	S2215Y
P-0000208-T02-IM5	MSK-IMPACT	S2215Y
P-0005214-T01-IM5	MSK-IMPACT	S2215Y
MEL-UKRV-Mel-20	Melanoma (Broad)	S2215Y
TCGA-BS-A0UF-01	Uterine (TCGA)	S2215Y
TCGA-BS-A0UV-01	Uterine (TCGA)	S2215Y
TCGA-BG-A0VX	Uterine (TCGA)	S2215Y
TCGA-CS-5396-01	Glioma (TCGA)	L2216P
HEC251-ENDOMETRIUM	CCLE	R2217W
TCGA-A6-4105-01	Colorectal (TCGA)	Q2223K
TCGA-CJ-4887-01	ccRCC (TCGA)	L2230V
SNU1196-BILIARY	CCLE	S2231W
KMH2-HAEMATOPOIE	CCLE	T2232I
CW2-LARGE-INTEST	CCLE	G2238D
TCGA-JW-A5VL-01	Cervical (TCGA)	W2239C
P-0000614-T01-IM3	MSK-IMPACT	W2239Fts*39
DS-bla-084	Bladder (MSKCC 2014)	P2241S
MSKCC-0296_R	Bladder (DFARBER_MSKCC 2014)	P2241S
TCGA-DK-A6B6-01	Bladder (TCGA)	P2241S
TCGA-JW-A5VL-01	Cervical (TCGA)	P2241S
TCGA-97-7554-01	Lung adeno (TCGA)	R2251Q
HEC1A-ENDOMETRIUM	CCLE	R2254M
SNU820-STOMACH	CCLE	H2265P
TCGA-75-5126-01	Lung adeno (TCGA)	R2266P
TCGA-34-5239-01	Lung squ (TCGA)	A2272S
TCGA-EB-A3Y7-01	Melanoma (TCGA)	A2272V
P-0005309-T01-IM5	MSK-IMPACT	Q2282P
TCGA-BR-8363-01	Stomach (TCGA)	T2294A
P-0001171-T01-IM3	MSK-IMPACT	D2298H
DS-bla-037	Bladder (MSKCC 2014)	E2311K
P-0001042-T01-IM3	MSK-IMPACT	A2325V
P-0003529-T01-IM5	MSK-IMPACT	V2330I
TCGA-AA-3666-01	Colorectal (TCGA)	I2333M
TCGA-B0-5691-01	Renal clear cell (TCGA)	L2334V
TCGA-HU-A4GU-01	Stomach (TCGA)	R2339_splice
L540-HAEMATOPOIE	CCLE	H2340R
TCGA-HB-A43Z-01	Sarcoma (TCGA)	S2342Y
NCIH446-LUNG	CCLE	M2345V
ESCC-148T	Esophagus sq (ICGC)	G2351E
LUAD-FH5PJ	Lung adeno (BROAD)	H2355R
S12-23181-TP-NT	CSCC (Dana-Farber)	G2359R
TCGA-E9-A54Y-01	Breast (TCGA)	R2368Q
HEC108-ENDOMETRIUM	CCLE (Novartis/Broad 2012)	R2368Q
P-0002079-T01-IM3	MSK-IMPACT	L2383F
P-0001042-T01-IM3	MSK-IMPACT	T2384I
TCGA-BH-A0HP-01	Breast (TCGA)	E2388Q
SW48-LARGE-INTEST	CCLE	V2389_splice
COSM51966	Kidney	V2406A
TCGA-A7-A5ZV-01	Breast (TCGA)	D2412H
H061142	Liver (AMC)	D2412V
TCGA-EK-A3GK-01	Cervical (TCGA)	E2419K
CLL147	CLL (BROAD)	A2420P
P-0003254-T01-IM5	MSK-IMPACT	A2420V
P-0004798-T01-IM5	MSK-IMPACT	A2420V
TCGA-FS-A4FC-06	Melanoma (TCGA)	A2420V
TCGA-ER-A42L-06	Melanoma (TCGA)	D2424N
ST486-HAEMATOPOI	CCLE	L2427R
TCGA-06-0122-01	GBM (TCGA)	L2427Q
TCGA-KN-8437-01	chRCC (TCGA)	L2427R
P-0005355-T01-IM5	MSK-IMPACT	L2427R
P-0005044-T01-IM5	MSK-IMPACT	L2427Q
P-0000839-T01-IM3	MSK-IMPACT	L2427Q
MOLT16-HAEMATOP	CCLE	R2430M
TCGA-G4-6322-01	Colorectal (TCGA)	R2441Q

Data were collected from the cBioPortal, MSKCC.

Author Queries

Journal: Nature

Paper: [nature17963](#)

Title: Overcoming mTOR resistance mutations with a new-generation mTOR inhibitor

Query	Query
<p>Author: Please check the wording of the following statement, which will appear online only.</p> <p>Reference</p> <p>K.M.S. is an inventor on patents related to MLN0128 held by the University of California San Francisco (UCSF), and sublicensed to Takeda Pharmaceuticals. N.R. and K.M.S. are consultants and M.O. is an employee at Takeda Pharmaceuticals Company Limited, which is conducting MLN0128 clinical trials. C.M., D.G.B., S.C. and T.K. are employees at AstraZeneca, which is conducting AZD2014 (mTOR kinase inhibitor) trials. K.M.S. and M.O. are inventors on a patent application related to RapaLink held by UCSF and licensed to Kura Oncology. K.M.S. is a shareholder in Kura Oncology, K.M.S. and N.R. are consultants to Kura Oncology.</p>	

For Nature office use only:

Layout	<input type="checkbox"/>	Figures/Tables/Boxes	<input type="checkbox"/>	References	<input type="checkbox"/>
DOI	<input type="checkbox"/>	Error bars	<input type="checkbox"/>	Supp info	<input type="checkbox"/>
Title	<input type="checkbox"/>	Colour	<input type="checkbox"/>	Acknowledgements	<input type="checkbox"/>
Authors	<input type="checkbox"/>	Text	<input type="checkbox"/>	Author contribs	<input type="checkbox"/>
Addresses	<input type="checkbox"/>	Methods	<input type="checkbox"/>	COI	<input type="checkbox"/>
First para	<input type="checkbox"/>	Received/Accepted	<input type="checkbox"/>	Correspondence	<input type="checkbox"/>
		AOP	<input type="checkbox"/>	Author corrx	<input type="checkbox"/>
		Extended Data	<input type="checkbox"/>	Web summary	<input type="checkbox"/>
				Accession codes link	<input type="checkbox"/>